IEICE TRANS. COMMUN., VOL.E95–B, NO.7 JULY 2012

PAPER

Accurate Image Expansion Method Using Range Points Based Ellipse Fitting for UWB Imaging Radar

Yoriaki ABE[†a)], ***Student Member***, **Shouhei KIDERA**[†], ***and*** **Tetsuo KIRIMOTO**[†], ***Members***

SUMMARY Ultra-wideband (UWB) pulse radars have a definite advantage in high-range resolution imaging, and are suitable for short-range measurements, particularly at disaster sites or security scenes where optical sensors are rarely suitable because of dust or strong backlighting. Although we have already proposed an accurate imaging algorithm called Range Points Migration (RPM), its reconstructible area is too small to identify the shape of an object if it is far from the radar and the size of the aperture is inadequate. To resolve this problem, this paper proposes a novel image expansion method based on ellipse extrapolation; it enhances extrapolation accuracy by deriving direct estimates of the observed range points distributed in the data space. Numerical validation shows that the proposed method accurately extrapolates part of the target boundary, even if an extremely small region of the target boundary is obtained by RPM.

key words: *UWB pulse radars, range points migration, ellipse fitting, image expansion*

1. Introduction

Ultra-wideband (UWB) pulse radars have great potential for short-range measurement with high range resolution, even in critical situations such as disaster or resource exploration scenes, where an optical measurement is rarely applicable owing to dust in the air or a high concentration of certain gases. In recent years, various radar imaging algorithms based on data synthesis, such as the synthetic aperture radar (SAR) algorithm [1], time-reversal algorithms [2], [3], and range migration methods [4], [5], have been proposed. However, their computational costs are often impractically large for applications such as robot or security sensing.

As a solution for this difficulty, the high-speed imaging algorithm, Shape Estimation Algorithm based on Boundary scattering transform (BST) and Extraction of Directly scattered waves (SEABED), achieves direct and nonparametric imaging based on reversible transforms between the time delay and target boundary [6]. However, the imaging accuracy of SEABED is severely degraded by the interference from multiple scattering centers, especially for multiple or complex-shaped targets. As a suitable approach for various target shapes or noisy situations, we have proposed an accurate imaging algorithm named Range Points Migration (RPM) [7], [8]. This algorithm directly converts a group of range points (a set of antenna locations and observed ranges) into a group of target points through accurate estimation of the direction of arrival. A notable feature of this method is that it guarantees a one-to-one correspondence between a range point and a target point, and there are various derivations of this method, such as complicated shape identification [9] or an internal imaging system for a target buried in a dielectric medium [10]. However, when the object is far from the observation site owing to the presence of obstacles such as rubble in a disaster area, the reconstruction area for RPM is too narrow to recognize whether an object is a human body or not due to the relatively inadequate aperture. This is a common problem inherent in all conventional approaches.

To enhance the imaging region of UWB radar, this paper proposes an accurate target boundary extrapolation method based on ellipse fitting. Since each part of human body, arm, leg or head, can be roughly approximated as ellipsoid, it is not an impractical assumption that the assumed target shape can be approximated by an aggregation of ellipsoids (ellipses in a 2-dimensional (2-D) model). To achieve this approximation, various ellipse extrapolation algorithms have been proposed. The algorithm proposed here is based on minimizing the square sum of the error distances between the estimated target points to the ellipse [11], [12]. This fitting issue is a type of nonlinear problem, and must be solved using a recursive approach, for which some effective methods have been developed in recent years [11], [12]. However, all the conventional approaches are too sensitive to the errors in the target points, especially if only a small region of the target boundary is reproduced.

To overcome this difficulty, the proposed method converts the problem of ellipse fitting in real space to that of range curve fitting in data space to enhance the extrapolation accuracy. Note that the range points observed from multiple ellipse targets have a complicated distribution in data space, and in general it is difficult to cluster them correctly. To avoid this difficulty, we focus on the unique relationship between a range point and a target point obtained using RPM. Thus, first in the proposed method, the range points in data space are classified into each target by applying a clustering algorithm to target points in real space obtained using RPM. Second, this method employs a range curve fitting for each set of clustered range points in data space to enable extrapolation of each ellipse target. A notable point of the proposed method is that it uses only the observed range data in the fitting process, while the RPM is used for clustering, and thus, it can enhance the fitting accuracy by avoiding the small errors that occur in the imaging process of RPM. Nu-

Manuscript received November 15, 2011.
Manuscript revised March 16, 2012.

[†]The authors are with Graduate School of Informatics and Engineering, The University of Electro-Communications, Chofu-shi, 182-8585 Japan.
a) E-mail: abe@secure.ee.uec.ac.jp

DOI: 10.1587/transcom.E95.B.2424

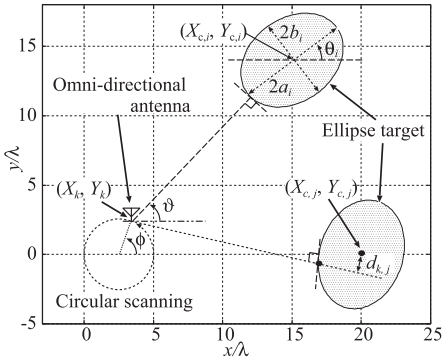

Fig. 1 System model.

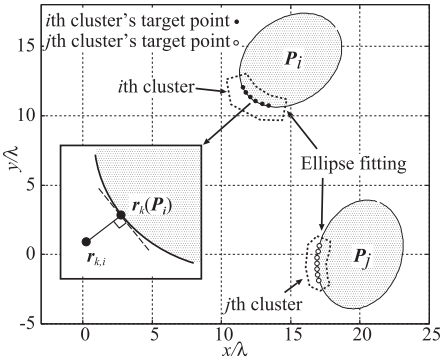

Fig. 2 Conventional scheme for ellipse extrapolation.

merical simulations, including 2-D and 3-D models, verify that even if an extremely small part of the ellipse boundary is reconstructed by the RPM, the proposed method accurately extrapolates the target boundary even in noisy situations.

2. System Model

Figure 1 shows the system model. The model assumes that targets have ellipse shapes with clear boundaries. It employs a mono-static radar system, where an omni-directional antenna is scanned along an arbitrary curve. We also assume that the propagation speed of the radio wave is known and constant. We use a mono-cycle pulse as the transmitting current, whose center wavelength is defined as λ. The space in which the targets and antenna are located is defined as real-space, and is expressed by the parameters (x, y). $s'(X, Y, t)$ is defined as the electric field received at the antenna location $(x, y) = (X, Y)$ at time t. $s(X, Y, t)$ is the output of the Wiener filter whose definition and filtering procedure are given in [7]. $s(X, Y, t)$ is converted to $s(X, Y, R')$ with $R' = c_0 t/2$, where c_0 is the speed of the radio wave. The group of the (X, Y, R) so-called range points are extracted from the local peaks of $s(X, Y, R')$ by:

$$\left.\begin{array}{l} \dfrac{\partial s(X,Y,R')}{\partial R'} = 0 \\ s(X,Y,R') \geq \alpha \max\limits_{R'} s(X,Y,R') \end{array}\right\}. \quad (1)$$

The parameter $\alpha(> 0)$ is empirically determined. The data space is defined as the space expressed by (X, Y, R).

3. Conventional Method

This section introduces one of the typical schemes for ellipse fitting using the target points estimated by the RPM in real space. Figure 2 shows the scheme for the conventional method. Here, we briefly explain this method. RPM assumes that a target point (x, y) exists on a circle with center (X, Y) and radius R, and then estimates the direction of arrival (ϑ in Fig. 1) by making use of the global characteristics of the observed range points [7], [8]. The optimum $\vartheta_{\rm opt}$ is calculated by

$$\vartheta_{\rm opt}(\boldsymbol{q}) = \arg \max_{0\leq\vartheta<2\pi} \sum_{i=1}^{2} \sum_{j=1}^{N_{\rm q}} s(X_j, Y_j, R_j) \times \exp\left[-\left\{ \frac{(X-X_j)^2 + (Y-Y_j)^2}{2\sigma_C^2} + \frac{\{\vartheta - \vartheta_i(\boldsymbol{q}, \boldsymbol{q_j})\}^2}{2\sigma_\vartheta^2} \right\} \right], \quad (2)$$

where $\boldsymbol{q} = (X, Y, R)$, $\boldsymbol{q}_j = (X_j, Y_j, R_j)$ and $N_{\rm q}$ is the number of the range points. The constants σ_C and σ_ϑ are empirically determined as in [7]. $\vartheta_i(\boldsymbol{q}, \boldsymbol{q}_j)$ denotes the angle from the x axis to the intersection points of the circles with parameters (X, Y, R) and (X_j, Y_j, R_j). Here, the two intersection points for each pair of circles are discriminated by the index i. The target point (x, y) is expressed as $x = X + R\cos\vartheta_{\rm opt}(\boldsymbol{q})$ and $y = Y + R\sin\vartheta_{\rm opt}(\boldsymbol{q})$.

Initially in this method, the target points produced by the RPM are obtained from the extracted range points (X, Y, R). To classify the estimated target points into multiple ellipse objects, each estimated target point is clustered according to its Euclidean distance [13], which is detailed in Sect. 4. Here, we define $\boldsymbol{P} \equiv (a, b, X_c, Y_c, \theta)$ as the parameters of the ellipse whose major axis is a, minor axis is b, the center of focal points is (X_c, Y_c), and angle from the x axis to the major axis is θ as shown in Fig. 1. This method then optimizes the parameter $\boldsymbol{P_i}$ for the ith cluster's ellipse by minimizing the following evaluation function:

$$\boldsymbol{P}_i^{\rm R} = \arg\min_{\boldsymbol{P}} \sum_{k=1}^{N_i} \| \boldsymbol{r}_{k,i} - \boldsymbol{r}_k(\boldsymbol{P}) \|^2, (i = 1, ..., C), \quad (3)$$

where $\boldsymbol{r}_{k,i} = (x_{k,i}, y_{k,i})$ denotes the location of the kth estimated target point in the ith cluster and $\boldsymbol{r}_k(\boldsymbol{P})$ denotes the location of the ellipse boundary point, which has a minimum distance to point $\boldsymbol{r}_{k,i}$. N_i denotes the total number of the estimated target points in the ith cluster, and C denotes the total number of clusters. Note that RPM imaging itself includes a small error, depending on the sampling interval of (X, Y), or the spatial distribution of the range points in data space. Thus, it is predicted that this method might guarantee the accuracy in ellipse fitting if a sufficient area of an ellipse boundary is reconstructed by RPM. However, if the estimated target points are distributed in a single small region of the target boundary, the accuracy of this method severely deteriorates because the extrapolation result is ex-

tremely sensitive to small errors of the target points caused by the RPM imaging in such cases. Although various algorithms for ellipse fitting have been proposed [11], [12], they basically utilize the estimated target points in real space and hence it is inherently difficult to resolve the problem mentioned above.

4. Proposed Method

To avoid the difficulty described in the previous section, we propose a novel image expansion method which exploits the observed range points for the ellipse extrapolation instead of using the estimated target points by the RPM. We focus here on a one-to-one correspondence between an estimated target point and a range point, which is the unique property of RPM [7]. This method first uses the target points produced by RPM only for the clustering of the range points, the distribution of which in data space is often very complicated in the case of multiple targets. The clustered range points are then employed for ellipse fitting, which is converted in data space. Figure 3 shows the scheme for the proposed method, where ϕ denotes the antenna location as shown in Fig. 1. In principle, an ellipse curve in real space is converted to a specified range curve in data space. Our method is basically impervious to RPM imaging error, and has significant potential to enhance the fitting accuracy because the range points should not include errors caused by the imaging process of RPM. In this method, $\boldsymbol{P}_i$ for the ith cluster is determined by:

$$\boldsymbol{P}_i^{\mathrm{D}} = \arg\min_{\boldsymbol{P}} \sum_{k=1}^{N_i} \left| \{R_{k,i} - R_k(\boldsymbol{P})\} \left(\frac{d_{k,i}^2}{\beta} + 1 \right) \right|^2, (i = 1, ..., C), \quad (4)$$

where $R_{k,i}$ denotes the range point corresponding to the kth estimated target point in the ith cluster and $R_k(\boldsymbol{P})$ denotes the orthogonal distance from (X_k, Y_k) to the ellipse expressed by $\boldsymbol{P}$. $d_{k,i}$ is the minimum distance from $(X_{c,i}, Y_{c,i})$ to the perpendicular line from the point (X_k, Y_k) to the ellipse $\boldsymbol{P}$, as shown in Fig. 1. The constant β is empirically determined. The weight function $(d_{k,i}^2/\beta + 1)$ in Eq. (4) prevents the deviation of the center of the focus of the ellipse from the actual center. The procedure for the proposed method is summarized as follows.

Step 1). A set of estimated target points $\mathcal{T}_{\mathrm{rpm}}$ is obtained by applying RPM to the observed range points.

Step 2). The two nearest estimated target points in $\mathcal{T}_{\mathrm{rpm}}$ are recursively combined as one cluster, until the distance for all pairs of clusters satisfies $D_{i,j} \geq \gamma$, where the constant γ is empirically determined. Here, $D_{i,j}$ is defined as

$$D_{i,j} = \frac{1}{n_i n_j} \sum_{k=1}^{n_i} \sum_{l=1}^{n_j} \| \boldsymbol{r}_{k,i} - \boldsymbol{r}_{l,j} \|, \quad (5)$$

where n_i and n_j denote the numbers of estimated target points in clusters C_i and C_j, respectively. $\boldsymbol{r}_{k,i}$ and $\boldsymbol{r}_{l,j}$ are the locations of estimated target points. All estimated target points in $\mathcal{T}_{\mathrm{rpm}}$ are then classified into multiple clusters.

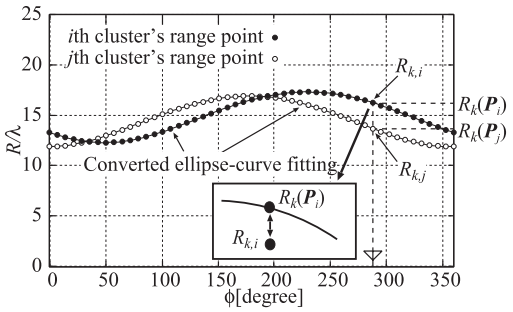

Fig. 3 Proposed scheme for ellipse extrapolation.

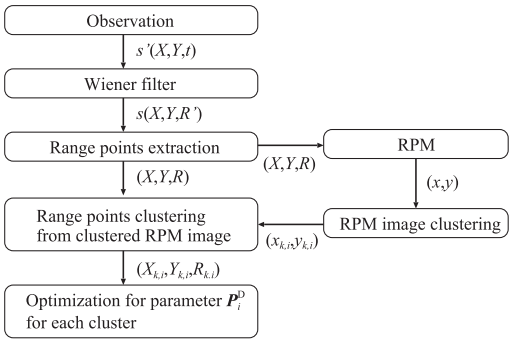

Fig. 4 Flowchart of the proposed method.

Step 3). The false clusters are removed, which satisfy:

$$\zeta \leq \kappa \max_i \zeta_i, \quad (6)$$

where $\zeta_i = \sum_{k=1}^{n_i} s(X_{k,i}, Y_{k,i}, R_{k,i})$ and the constant κ is empirically determined. Based on the fact that the actual cluster has a larger number of estimated target points compared with the cluster attribute to noises, this procedure removes such a noisy cluster.

Step 4). For each cluster, the optimal parameter $\boldsymbol{P}^{\mathrm{D}}$ is determined using Eq. (4).

Figure 4 illustrates the flowchart of the proposed method. While the estimated target points obtained by the RPM are employed for clustering or distance measurement for an ellipse in Step 2, the fitting process itself is completed without RPM imaging. Therefore, the fitting accuracy of this method depends only on the range errors and should be a substantial improvement over that of the conventional approach.

5. Performance Evaluation in Numerical Simulation

This section investigates the performance of each method. Six ellipse targets are assumed in this case. An omnidirectional antenna scans along a circle whose center is

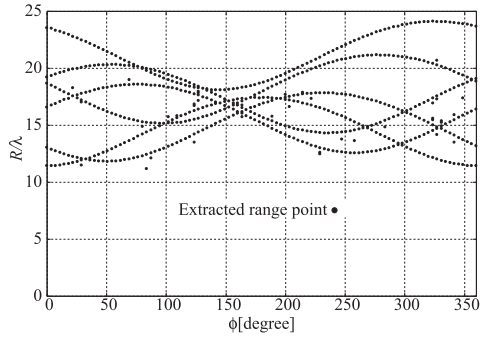

Fig. 5 Extracted range points for six ellipses at S/N = 40 dB.

$(x, y) = (2.5\lambda, 0)$ and radius is 2.5λ. The received signal $s'(X, Y, t)$ is created as follows,

$$s'(X, Y, t) = \sum_{i=1}^{N_T} \frac{1}{\sqrt{2r_i}} s_{tr}\left(t - \frac{2r_i}{c_0}\right), \quad (7)$$

where $s_{tr}(t)$ is the transmitted signal, N_T is the total number of targets and r_i is the minimum distance between (X, Y) and the target. Equation (7) denotes a simplified geometrical optics approximation. While in a realistic model, the scattered waveform is slightly distorted from the transmitted one [14], in the case of a much larger size target with smooth curves than the wavelength, this deformation is negligible, and this effect is not considered here. Gaussian white noise is added to the received signals, and the signal-to-noise ratio (S/N) is 40 dB in this case. Here, the S/N is defined as the ratio of peak instantaneous signal power to the averaged noise power after applying the matched filter. Although the discussed S/N seems to be extremely high, the definition of the S/N considers the locality both in the frequency domain and in the time domain in order to estimate UWB pulse power with a most strict criterion, and [7] indicates that the actual UWB radar system can achieve this level of S/N.

Figure 5 shows the extracted range points (X, Y, R), where ϕ denotes the angle as shown in Fig. 1. α is set at 0.3. Note that if α is set to a smaller value, range points derived from a noisy component can be extracted, which causes false images in RPM. On the contrary, if α is set to a larger value, an actual range point which has relatively small amplitude is not extracted, which causes the misdetection of an actual target. The parameter study of α is investigated in [7]. The simulated annealing algorithm [15] is employed to obtain a global optimum in Eq. (3) or (4), where the Levenberg Marquardt method is sequentially involved for local optimization. Figure 6 shows the estimated target points by the RPM after the clustering. It shows that only a small region of the target boundaries can be reconstructed in this case and false images are produced owing to additive random noises. Figure 7 shows the ellipses estimated using the conventional method described in Sect. 3. This example shows that regardless of a relatively high S/N, the accuracy of the conventional method deteriorates mainly due to the small errors of RPM imaging. On the other hand, Fig. 8 shows the ellipses estimated using the proposed method.

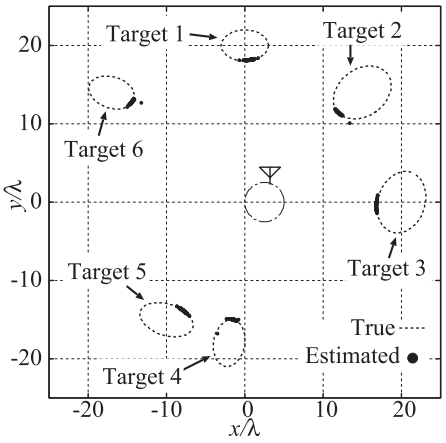

Fig. 6 Estimated target points obtained by the RPM after the clustering at S/N = 40 dB.

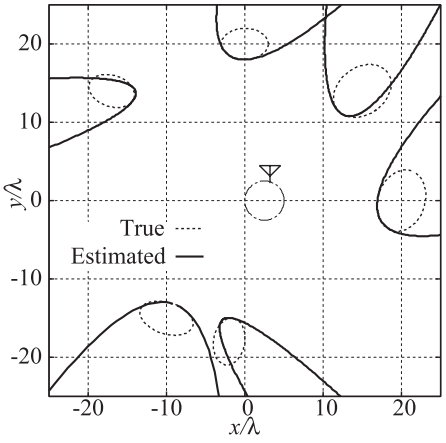

Fig. 7 Estimated ellipses by the conventional method at S/N = 40 dB.

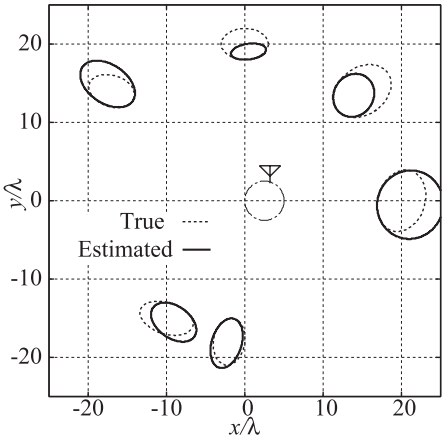

Fig. 8 Estimated ellipses by the proposed method at S/N = 40 dB.

The following parameters are set: $\beta = 60\lambda^2, \gamma = 3\lambda$ and $\kappa = 0.4$. This result shows that the proposed method extrapolates the target image more accurately than the conventional method, avoiding the effect of errors in RPM imaging. Here, it should be noted that the value of β is adjusted

to add about 50 % to the weight $(d_{k,i}^2/\beta + 1)$ in Eq. (4), when the distance between the true center and estimated center of the focal points approaches 5λ. The value of γ is chosen under the assumption that the size of the actual ellipse target is more than 3λ. The value of κ is chosen so that the cluster attributed to a noisy component can be adequately eliminated. While these parameters are determined when considering the assumed target size, S/N or observation scale, a more systematic way to determine them would be required, and is left to future study.

Despite the proposed method enhancing the fitting accuracy compared to the conventional method as shown in previous results, there is still a certain error in ellipse estimation, because the evaluation function in Eq. (4) is still sensitive to small range errors. To emphasize the extrapolated boundary of the targets from a statistical viewpoint, another approach for the image expression is introduced as follows. First, the following function $S_i(x, y)$, that expresses the accumulated ellipse boundaries obtained from the sequential results of simulated annealing, is introduced as

$$S_i(x, y) = \sum_{m=1}^{M_i} \delta(x - \hat{x}_{m,i}, y - \hat{y}_{m,i}), \tag{8}$$

where

$$\delta(x, y) = \begin{cases} 1 & (x = 0,\ y = 0) \\ 0 & (\text{otherwise}) \end{cases}, \tag{9}$$

holds. $\hat{x}_{m,i}$ and $\hat{y}_{m,i}$ are the x and y coordinates that satisfy $f(\hat{x}_{m,i}, \hat{y}_{m,i}; \boldsymbol{P_i}) = 0$, respectively, where $\boldsymbol{P}_i$ is the sequential output of the simulated annealing when the value in Eq. (4) becomes less than a predetermined threshold. M_i is the number of the obtained $\boldsymbol{P}_i$. Here, $f(x, y; \boldsymbol{P})$ expresses a function of an ellipse in general form as

$$f(x, y; \boldsymbol{P}) = \left\{ \frac{(x - X_c)\cos\theta + (y - Y_c)\sin\theta}{a} \right\}^2 + \left\{ \frac{-(x - X_c)\sin\theta + (y - Y_c)\cos\theta}{b} \right\}^2 - 1. \tag{10}$$

The focused region of the ellipse boundaries obtained from the results of the simulated annealing is then extracted as the probable target image $I_i(x, y)$, which is defined as

$$I_i(x, y) = \begin{cases} 1 & (S_i(x, y) \geq \eta \max\limits_{(x,y)} S_i(x, y)) \\ 0 & (\text{otherwise}) \end{cases}. \tag{11}$$

The constant η is empirically determined and set to 0.5 in this simulation to emphasize the spatial region, where a large number of ellipse boundaries are accumulated. Note that to eliminate outlying results, η should to some extent maintain a higher value. Figure 9 shows the extrapolated target points using the conventional method. Here, the real space is gridironed and the extrapolated target point is defined as the grid point that satisfies $I_i(x, y) = 1$. The figure shows that the accuracy of the conventional method is still insufficient. However, Fig. 10, illustrating the extrapolated target points obtained by the proposed method, shows that a large part of the ellipse boundary is accurately extrapolated, which is barely evident from the original RPM image.

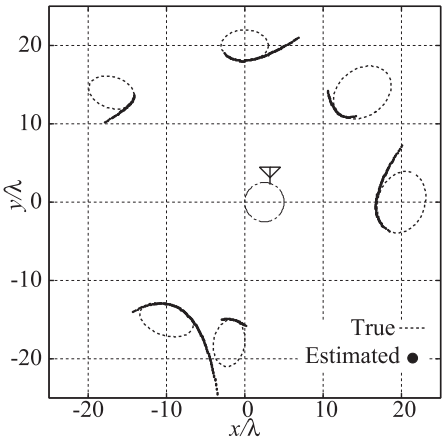

Fig. 9 Extrapolated target points $I(x_i, y_i)$ obtained by the conventional method at S/N = 40 dB.

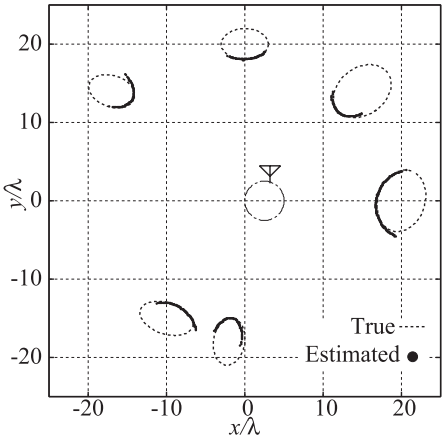

Fig. 10 Extrapolated target points $I(x_i, y_i)$ obtained by the proposed method at S/N = 40 dB.

In addition, the examples of both methods in the lower S/N situation are investigated. Figures 11, 12 and 13 show that the estimated target points using the RPM and the extrapolated target points obtained by the conventional and proposed method, respectively and the S/N is around 20 dB. The figures show that while the accuracy of the conventional method deteriorates for the same reason as in the higher S/N case, the proposed method holds a high accuracy even in lower S/N and reconstructs a wider area of the target boundaries than that produced by the RPM.

For a quantitative evaluation of the accuracy, ϵ is introduced as

$$\epsilon = \frac{\sum_{i=1}^{N} \min\limits_{\boldsymbol{x}} \| \boldsymbol{x} - \boldsymbol{x}_e^i \|}{N}, \tag{12}$$

where $\boldsymbol{x}$ and $\boldsymbol{x}_e^i$ express the location of the true target point and the extrapolated target point, respectively. N is the total

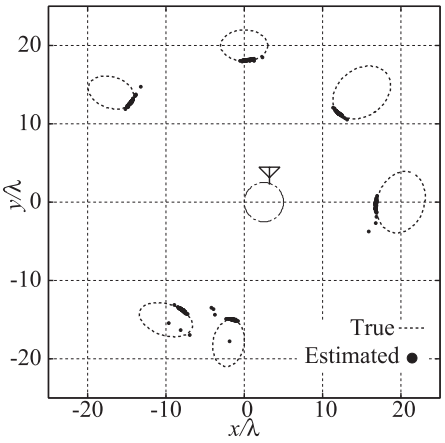

Fig. 11 Estimated target points obtained by the RPM after the clustering at S/N = 20 dB.

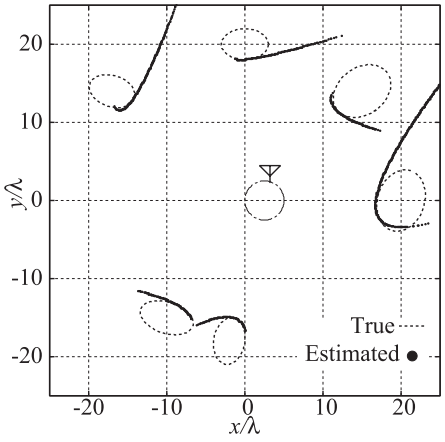

Fig. 12 Extrapolated target points $I(x_i, y_i)$ obtained by the conventional method at S/N = 20 dB.

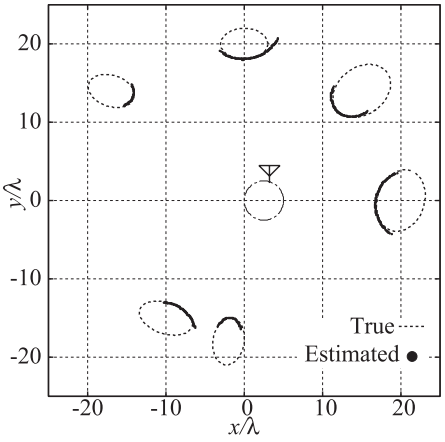

Fig. 13 Extrapolated target points $I(x_i, y_i)$ obtained by the proposed method at S/N = 20 dB.

number of $\boldsymbol{x}_e^i$. Tables 1 and 2 show the comparison of ϵ/λ between the conventional and proposed method, for each target case, numbered as in Fig. 6, at S/N = 40 dB and 20 dB, respectively. The tables indicate that for all targets, the values of ϵ/λ for the proposed method are significantly lower than those of the conventional method for high and low S/N cases. Moreover, Fig. 14 shows the relationship between ϵ/λ and the S/N of the conventional method and the proposed method for targets 3 and 4. The figure shows that the value of ϵ/λ for the proposed method is considerably lower than that of the conventional method for all S/N, and this result validates the significant robustness of our proposed extrapolation method.

Table 1 Value of ϵ/λ for each target at S/N = 40 dB.

Target	1	2	3	4	5	6
Conventional	0.836	0.157	0.491	0.161	1.728	0.411
Proposed	0.031	0.062	0.103	0.079	0.111	0.123

Table 2 Value of ϵ/λ for each target at S/N = 20 dB.

Target	1	2	3	4	5	6
Conventional	2.464	0.578	3.310	0.580	0.308	3.550
Proposed	0.280	0.053	0.081	0.044	0.083	0.066

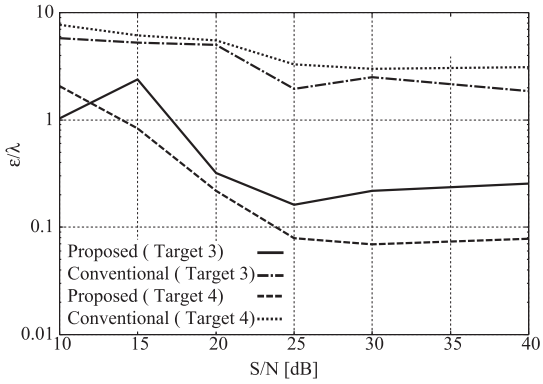

Fig. 14 Relationship between ϵ/λ and S/N for the conventional and proposed methods.

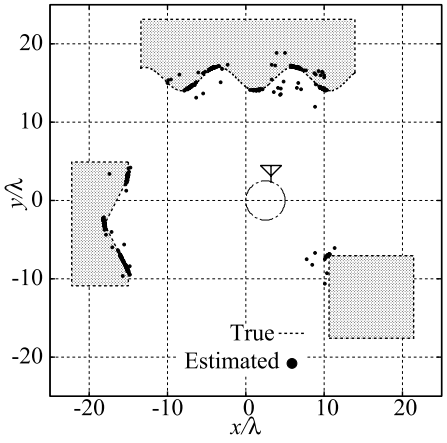

Fig. 15 Estimated target points obtained by the RPM after the clustering at S/N = 30 dB in the case of not ellipse objects.

For reference, one example including various target shapes not close to the ellipse, is investigated. Figures 15 and 16 show the estimated target points using RPM after clustering and the extrapolated target points obtained by the

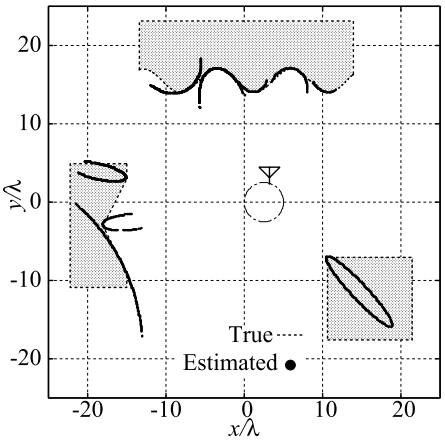

Fig. 16 Extrapolated target points $I(x_i, y_i)$ obtained by the proposed method at S/N = 30 dB in the case of not ellipse objects.

proposed method. The S/N here is around 30 dB. Figure 16 shows that while the extrapolation accuracy of the proposed method for smooth curves is relatively high, this accuracy significantly degrades for the region around convex or concave edges. This result also indicates that the extrapolation outputs around a concave shape are located on the opposite side of the actual boundary. This is an essential problem of ellipse specified extrapolation. The expansion of this method for concave or a more complicated target is an important task, which will be addressed in our future studies.

6. 3-D Extension

6.1 System Model

This section extends both the conventional and proposed method to the 3-D problem. Figure 17 shows the system model for the 3-D problem. The target model, antenna, and transmitted signal are the same as those assumed in the 2-D problem. The antenna is scanned on the plane, $z = 0$. The real space is expressed by the parameter (x, y, z). We assume $z \geq 0$ for simplicity. $s'(X, Y, t)$ is defined as the electric field received at the antenna location $(x, y, z) = (X, Y, 0)$. The output of the Wiener filter $s(X, Y, R')$ is obtained by the same procedure as described in Sect. 2. The group of range points (X, Y, R) are extracted by using the same criteria as in Eq. (1). We define $\boldsymbol{P}^{3d} = (a, b, c, X_c, Y_c, Z_c, \theta, \varphi, \psi)$ as parameters of the ellipsoid whose equatorial radii (along the x and y axes) are a and b, polar radius (along the z axis) is c, the center of focal points is (X_c, Y_c, Z_c), and the yaw, pitch and roll angle are θ, φ and ψ.

The conventional and proposed methods are easily extended to the 3-D model, where each parameter in Eqs. (3) and (4) is modified in terms of the estimated target points, the range points and the ellipsoid parameter.

6.2 Performance Evaluation in Numerical Simulation

This section presents examples for the conventional and proposed method. Four ellipsoid targets are assumed in this case. The received signals are observed at 441 ($= 21 \times 21$) locations for $0.0 \leq x, y \leq 5.0\lambda$, where the 3-D extension of Eq. (7) is employed. Figure 18 shows the estimated target points by the RPM. All parameters, $\alpha, \beta, \gamma, \kappa$ and η, are set to the same values as in Sect. 5. The S/N is 30 dB in this case. Figure 19 shows the extrapolated target points by using the conventional method, where $I_i(x, y, z)$ is naturally extended with $\delta(x, y, z)$ and the equation of the ellipsoid. The figure shows that the accuracy of the conventional method severely degrades for the same reason as discussed in the 2-D case. On the contrary, Fig. 20 shows the extrapolated target points

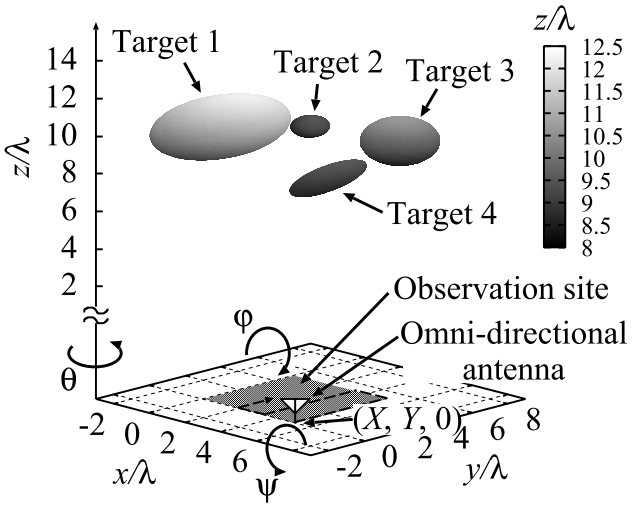

Fig. 17 System model in 3-D problem.

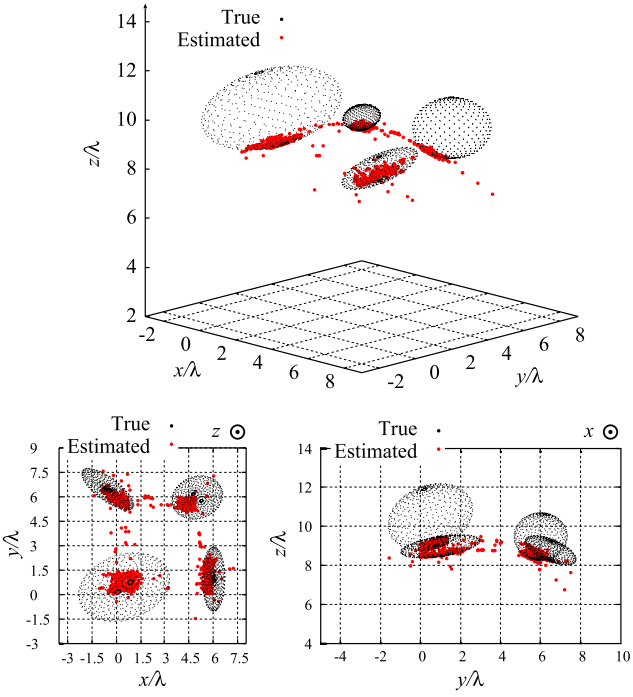

Fig. 18 Estimated target points obtained by the RPM at S/N = 30 dB.

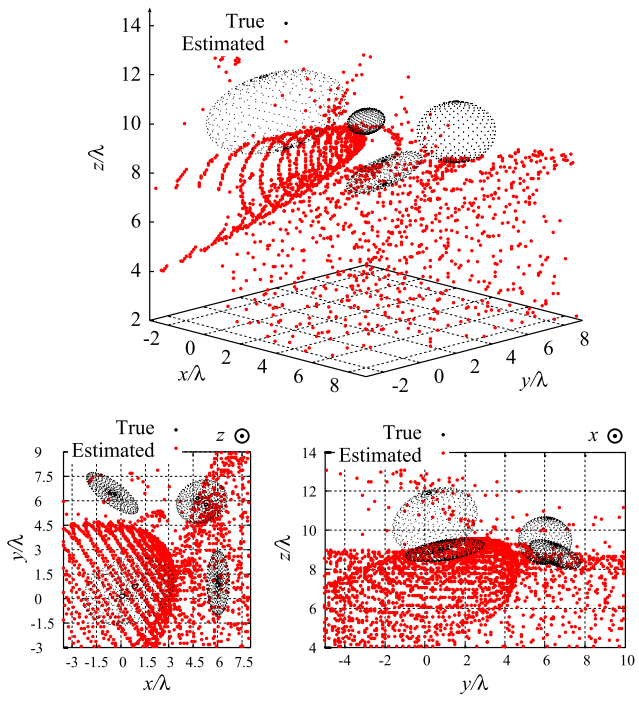

Fig. 19 Extrapolated target points $I(x_i, y_i, z_i)$ obtained by the conventional method at S/N = 30 dB.

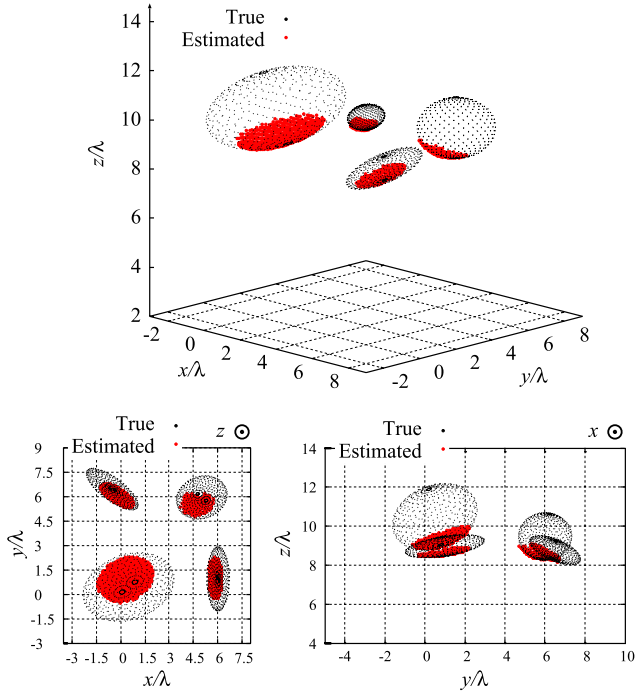

Fig. 20 Extrapolated target points $I(x_i, y_i, z_i)$ obtained by the proposed method at S/N = 30 dB.

by using the proposed method, and shows that our method accurately extrapolates a large part of the ellipsoid boundary compared with those obtained by the original RPM and the conventional method. Table 3 shows the comparison of ϵ/λ between the conventional and proposed methods, for each target case, numbered as in Fig. 17. The table indicates that the values of ϵ/λ of the proposed method are significantly lower than those of the conventional method for all targets. The calculation time of the proposed method after the clustering is about 2600 seconds when processed on a Xeon 2.4 GHz processor.

Table 3 Value of ϵ/λ for each target at S/N 30 dB.

Target	1	2	3	4
Conventional	2.191	2.294	7.632	10.098
Proposed	0.035	0.042	0.023	0.048

7. Conclusion

This paper described the target-boundary extrapolation scheme as a conventional method that employs ellipse fitting with target points obtained using RPM. We proposed a novel extrapolation by exploiting the observed range points for ellipse fitting, which are clustered into each ellipse object using the estimated target points obtained from RPM. Although estimated target points are used in classifying the range points in target clustering, this method is basically impervious to the accuracy of RPM imaging, and hence enhances the fitting accuracy compared to the conventional approach. Numerical simulations exemplify that while the accuracy of the conventional method critically deteriorates owing to small estimation errors of estimated target points, the proposed method accurately expands the parts of the multiple ellipse boundaries, even if only a small region of the target boundary is reproduced by the original RPM method. We also extended both the conventional and proposed methods to a 3-D model, where each approach is naturally modified. It was confirmed that the proposed method accurately reconstructs the wider areas of the multiple ellipsoid target boundaries compared with that produced by the RPM, even for 3-D targets. In future work, we will deal with an arbitrary target shape, where the multiple scattering components are appropriately considered by introducing a false image suppression scheme.

Acknowledgment

This work is supported in part by the Grant-in-Aid for Scientific Research (B) (Grant No. 22360161) and the Grant-in-Aid for Young Scientists (B) (Grant No. 23760364), promoted by Japan Society for the Promotion of Science (JSPS), and the Research Grant promoted by CASIO Science Promotion Foundation.

References

[1] D.L. Mensa, G. Heidbreder, and G. Wade, "Aperture synthesis by object rotation in coherent imaging," IEEE Trans. Nucl. Sci., vol.27, no.2, pp.989–998, April 1980.
[2] A.J. Devaney, "Time reversal imaging of obscured targets from multistatic data," IEEE Trans. Antennas Propag., vol.53, no.5, pp.1600–1610, May 2005.

[3] E.A. Marengo, F.K. Gruber, and F. Simonetti, "Time-reversal MUSIC imaging of extended targets," IEEE Trans. Image Process., vol.16, no.8, pp.1967–1984, Aug. 2007.
[4] J. Song, Q.H. Liu, P. Torrione, and L. Collins, "Two-dimensional and three dimensional NUFFT migration method for landmine detection using ground-penetrating radar," IEEE Trans. Geosci. Remote Sens., vol.44, no.6, pp.1462–1469, June 2006.
[5] F. Soldovieri, A. Brancaccio, G. Prisco, G. Leone, and R. Pieri, "A Kirchhoff-based shape reconstruction algorithm for the multimonostatic configuration: The realistic case of buried pipes," IEEE Trans. Geosci. Remote Sens., vol.46, no.10, pp.3031–3038, Oct. 2008.
[6] T. Sakamoto and T. Sato, "A target shape estimation algorithm for pulse radar systems based on boundary scattering transform," IEICE Trans. Commun., vol.E87-B, no.5, pp.1357–1365, May 2004.
[7] S. Kidera, T. Sakamoto, and T. Sato, "Accurate UWB radar 3-D imaging algorithm for complex boundary without range points connections," IEEE Trans. Geosci. Remote Sens., vol.48, no.4, pp.1993–2004, April 2010.
[8] Y. Abe, S. Kidera, and T. Kirimoto, "Accurate and Omni-directional UWB radar imaging algorithm with RPM method extended to curvilinear scanning model," IEEE Geosci. Remote Sensing Lett., vol.9, no.1, pp.144–148, Jan. 2012.
[9] R. Salman and I. Willms, "3D UWB radar super-resolution imaging for complex objects with discontinous wavefronts," Proc. IEEE Intl. Conf. on Ultra Wideband 2011, pp.2162–6588, Sept. 2011.
[10] K. Akune, S. Kidera, and T. Kirimoto, "Fast and accurate imaging algorithm for targets buried in dielectric medium for UWB radars," Proc. General Assembly and Scientific Symposium, 2011 XXXth URSI, Aug. 2011.
[11] S.J. Ahn, W. Rauh, and H.J. Warnecke, "Least-squares orthogonal distances fitting of circle, sphere, ellipse, hyperbola, and parabola," Pattern Recognit., vol.34, no.12, pp.2283–2303, Dec. 2001,
[12] A. Atieg and G.A. Watson, "A class of methods for fitting a curve or surface to data by minimizing the sum of squares of orthogonal distances," J. Computational and Applied Mathematics, vol.158, no.2, pp.277–296, Sept. 2003.
[13] R.R. Sokal and C.D. Michener, "A statistical method for evaluating systematic relationships," University of Kansas Science Bulletin, vol.28, pp.1409–1438, 1958.
[14] S. Kidera, T. Sakamoto, T. Sato, and S. Sugino, "An accurate imaging algorithm with scattered waveform estimation for UWB pulse radars," IEICE Trans. Commun., vol.E89-B, no.9, pp.2588–2595, Sept. 2006.
[15] S. Kirkpatrick, C.D. Gelatt, and M.P. Vecchi, "Optimization by simulated annealing," Science, no.220, pp.671–680, 1983.

Yoriaki Abe received his B.E. degrees in Electronic Engineering from University of Electro-Communications in 2010. He is currently studying for an M.M. degree at Graduate School of Informatics and Engineering, University of Electro-Communications. His current research interest is advanced radar signal processing for UWB radar systems.

Shouhei Kidera received his B.E. degree in Electrical and Electronic Engineering from Kyoto University in 2003 and M.I. and Ph.D. degrees in Informatics from Kyoto University in 2005 and 2007, respectively. He is an assistant professor in Graduate School of Informatics and Engineering, University of Electro-Communications, Japan. His current research interest is in advanced signal processing for the near field radar, UWB radar. He is a member of the Institute of Electrical and Electronics Engineering (IEEE) and the Institute of Electrical Engineering of Japan (IEEJ).

Tetsuo Kirimoto received the B.S. and M.S. and Ph.D. degrees in Communication Engineering from Osaka University in 1976, 1978 and 1995, respectively. During 1978–2003 he stayed in Mitsubishi Electric Corp. to study radar signal processing. From 1982 to 1983, he stayed as a visiting scientist at the Remote Sensing Laboratory of the University of Kansas. From 2003 to 2007, he joined the University of Kitakyushu as a Professor. Since 2007, he has been with the University of Electro-Communications, where he is a Professor at the Graduate School of Informatics and Engineering. His current study interests include digital signal processing and its application to various sensor systems. Prof. Kirimoto is a senior member of IEEE and a member of SICE (The Society of Instrument and Control Engineers) of Japan.